Breakdown of the correspondence between the real-complex and delocalization-localization transitions in non-Hermitian quasicrystals

Wen Chen [1], Shujie Cheng,[1,*] Ji Lin [1], Reza Asgari,[2,1] and Gao Xianlong [1,†]
[1]*Department of Physics, Zhejiang Normal University, Jinhua 321004, China*
[2]*School of Physics, Institute for Research in Fundamental Sciences (IPM), Tehran 19395-5531, Iran*

(Received 28 August 2022; accepted 15 October 2022; published 31 October 2022)

The correspondence between the real-complex transition in energy and delocalization-localization transition is well established in a class of Aubry-André-Harper model with exponential non-Hermitian on-site potentials. In this paper, we study a generalized Aubry-André model with off-diagonal modulation and non-Hermitian on-site potential. We find that, when there exists an incommensurate off-diagonal modulation, the correspondence breaks down, although the extended phase is maintained in a wide parameter range of the strengths of the on-site potential and the off-diagonal hoppings. An additional intermediate phase with a non-Hermitian mobility edge emerges when the off-diagonal hoppings become commensurate. This phase is characterized by the real and complex sections of the energy spectrum corresponding to the extended and localized states. In this case, the aforementioned correspondence reappears due to the recovery of the $\mathcal{PT}$ symmetry.

DOI: 10.1103/PhysRevB.106.144208

I. INTRODUCTION

Anderson localization, an active topic in the condensed matter field, tells us that the random disorder fails the diffusion of the wave packets, and leads to the localization of the particle [1–4]. In addition, the quasidisorder systems, exemplified by the Aubry-André-Harper (AAH) model [5,6], are of a similar localized phenomenon but with a transition between extended and localized states with the increase of the disordered external potential in a one-dimensional system, which appears only in a three-dimensional system of random disorder [2]. Owing to the rich phase transitions in the quasidisordered systems, there is growing interest both in the theoretical study of the AAH system and its extensions [7–13] as well as their experimental realizations in the photonic crystals [14–17] and in the ultracold atomic systems [18–20].

The AAH model has been extended in numerous ways, such as by including long-range hopping, p-wave pairs, and off-diagonal modulations, which result in a variety of exotic phenomena. The long-range hopping term [21] or some specific form of the on-site potentials [22] results in the single-particle mobility edges. The off-diagonal terms lead to the presence of critical states in a large parameter space, and brings up the phase-transition structure of the extended-localized-extended states [23,24]. Additionally, the phase diagram of the system will change depending on whether the nondiagonal modulation is commensurate or incommensurate.

Further extensions to the AAH model apply to the non-Hermitian systems [22,25–40], where the corresponding localization, mobility edge, and topological properties usually discussed in the Hermitian system are given new properties. The inclusion of nonreciprocal hoppings or complex on-site potentials are theoretically the two ways to incorporate non-Hermiticity into disordered systems [41]. Theoretical investigation shows that there are synchronous real-complex transition and delocalization-localization transitions in the presence of the on-site complex potential [29,42], long-range hoppings [21,22,43], and the antisymmetric hops [35–38]. The combination of p-wave pairings and non-Hermitian quasidisorder is another important paradigm to understand the topological properties of quasiperiodic systems [44], and an unconventional real-complex transition is found in the non-Hermitian quasiperiodic lattice.

We should point out that Longhi [29] systematically examined the relationship between the real-complex transition in energy and the delocalization-localization transition in a class of AAH models with non-Hermitian exponential potentials and discovered that the extended states correspond to the real energies and the localized ones to the complex energies. A key question is whether such a correspondence is robust against the off-diagonal incommensurate and commensurate hoppings. In this paper, we study a generalized AAH model with off-diagonal modulation and non-Hermitian on-site potential and find that, for the AAH model with exponential non-Hermitian potential, such a well-established correspondence depends on the commensurate off-diagonal hoppings and breaks down when there exists an incommensurate off-diagonal modulation.

The rest of this paper is organized as follows. In Sec. II, we propose the generalized non-Hermitian AA model with two different types of off-diagonal hoppings. In Sec. III, we are devoted to investigating the localization transition and the properties of the energy spectra under the interplay of the incommensurate modulation and non-Hermitian on-site potential. In Sec. IV, we study the delocalization-localization

*chengsj@zjnu.edu.cn
†gaoxl@zjnu.edu.cn

 ©2022 American Physical Society

transition and analyze the properties of the energy spectra under commensurate off-diagonal hoppings. We make a summary in Sec. V.

II. MODEL AND HAMILTONIAN

The interplay of non-Hermiticity and quasidisorder gives rise to new perspectives for the Anderson localization transitions. In this paper, we consider a generalized AAH model with off-diagonal modulation and non-Hermitian on-site potential. The Hamiltonian is described as

$$\hat{H} = \sum_{n}^{L-1}[t_n(\hat{c}_{n+1}^{\dagger}\hat{c}_n + \text{H.c.})] + \sum_{n} V_n \hat{c}_n^{\dagger}\hat{c}_n, \tag{1}$$

where L is the length of the lattice, and $c_n(c_n^{\dagger})$ denotes the fermion annihilation (creation) operator at site n. The nearest-neighbor hopping amplitude t_n and on-site potential V_n are given by

$$\begin{aligned} t_n &= t + \lambda\cos(2\pi b_1 n + \phi_1), \\ V_n &= V\exp[i(2\pi b_2 n + \phi_2)], \end{aligned} \tag{2}$$

where λ and V denote the modulation amplitudes in the hopping term and on-site complex potential, respectively. An irrational or rational number, b_1, is selected, to represent the incommensurate or commensurate potential, respectively. For the on-site complex incommensurate modulation b_2, we discuss in this paper the irrational number $b_2 = (\sqrt{5}-1)/2$. ϕ_1 and ϕ_2 are the extra phases varying from 0 to 2π. In this work, we set t as the energy unit, and choose $\phi_1 = \phi_2 \equiv 0$ without loss of generality. (Although the phase boundary changes for different values of phases, the main physics remains the same).

In the limit of $\lambda = 0$, our model reduces to a non-Hermitian AAH model [29], in which exists a well-defined correspondence between the real-complex transition in energy and the delocalization-localization transition, supported by both an analytical and a numerical study. Namely, the real energies correspond to the extended states and the complex ones correspond to the localized states. In the limit of $V = 0$, our model is the one of the limits of the off-diagonal AAH model including both incommensurate and commensurate modulations [24], which displays an extended-critical transition for $b_1 = (\sqrt{5}-1)/2$; and regardless of the strength of the modulation, it maintains the extended phases for $b_1 = 1/2$. For the system of the non-Hermitian on-site potential, we are interested in determining whether the delocalization-localization transition still exists and whether the aforementioned connection is resistant to off-diagonal modulations (see the Appendix for the systems' symmetries).

III. INCOMMENSURATE MODULATION CASE

First, we study the phase properties of the model with incommensurate modulation $b_1 = (\sqrt{5}-1)/2$. The extended, localized, or critical feature of a specific wave function can be characterized by the inverse participation ratio (IPR) [45,46]

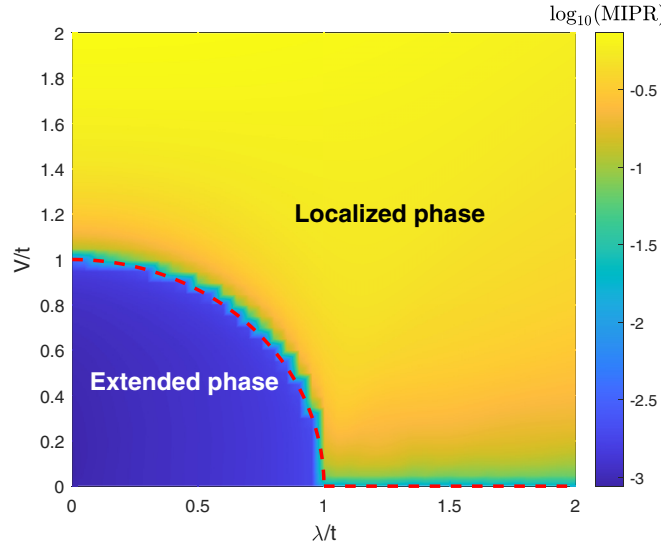

FIG. 1. Phase diagram for the incommensurate modulation case presents the $\log_{10}$(MIPR) as functions of V/t and λ/t with the system size $L = 1597$. The red dashed line is the phase boundary based on Eq. (1), separating the extended phase from the localized one. The color bar is for the value of $\log_{10}$(MIPR).

with

$$\text{IPR}^j = \frac{\sum_{n=1}^{L}|\psi^{(j)}(n)|^4}{\sum_{n=1}^{L}|\psi^{(j)}(n)|^2}, \tag{3}$$

corresponding to IPR $\to$ 1, IPR $\to$ 0, and 0 < IPR < 1, in the thermodynamic limit, respectively, where $\psi^{(j)}$ means the wave function of the jth eigenstate. Averaging the IPR over all the wave functions, that is, the mean inverse participation ratio (MIPR) with MIPR $= \sum_{j=1}^{L}\text{IPR}^{(j)}/L$ will be used to analyze the global characteristics of the system.

Having calculated the logarithm of the MIPR for a large system size ($L = 1597$), we obtain the phase diagram in the λ-V parameter space (see Fig. 1). Intuitively, the phase diagram consists of two different phases separated by the quarter circle (shown with a red dashed line and will be discussed later). In the parameter region surrounded by the inner quarter circle, the $\log_{10}$(MIPR) is visibly less than -1, meaning that the MIPR is approaching 0 in the large system size, indicating a delocalized phase. On the contrary, outside the quarter circle, the $\log_{10}$(MIPR) tends to 0, with the MIPR approaching 1, implying a localized phase. In particular, the $\log_{10}$(MIPR) is nearly equal to -1 on the phase boundary. This means that it is possible the wave functions will be critical at these parameter points. The difference between the phases can be reflected by the spatial distributions of wave functions as well.

In Figs. 2(a), 2(b), and 2(c), we display the spatial distributions of the three representative eigenstates $\psi^{(1000)}$ chosen from the above three phase areas with $(\lambda, V) = (1.5t, 1.5t)$, $(1.5t, 0t)$, and $(0.5t, 0.5t)$, respectively. We see that the wave function is localized for $(\lambda, V) = (1.5t, 1.5t)$, whereas it is extended for $(\lambda, V) = (0.5t, 0.5t)$. The wave function is neither extended nor localized for $(\lambda, V) = (1.5t, 0t)$, showing the multifractal structure with critical characteristics.

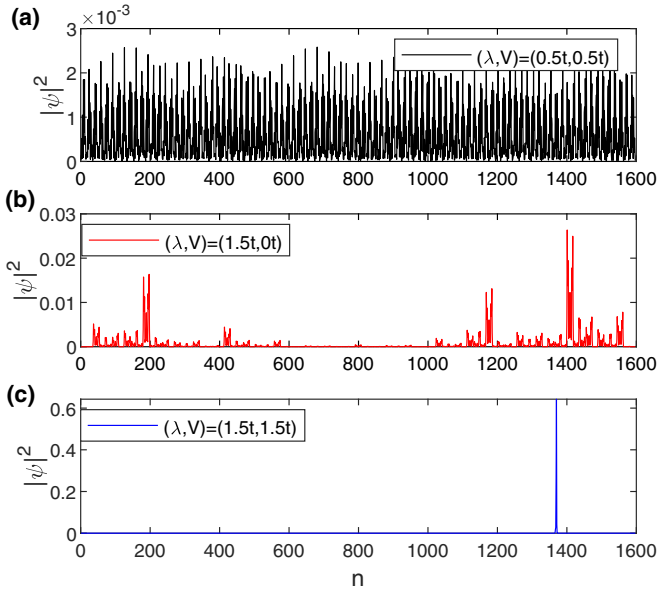

FIG. 2. The representative wave functions ψ_{1000}. (a) $(\lambda, V) = (0.5t, 0.5t)$ in the extended phase. (b) $(\lambda, V) = (1.5t, 0t)$ in the critical phase. (c) $(\lambda, V) = (1.5t, 1.5t)$ in the localized phase. The system size is $L = 1597$.

Furthermore, we locate the phase boundary when $\lambda < 1$ employing the $\log_{10}$(MIPR). In Fig. 3(a), we present $\log_{10}$(MIPR) as a function of $r = \sqrt{V^2 + \lambda^2}$ for various $\theta = \text{atan}(V/\lambda) \in [0, \pi/2]$ with the system size $L = 1597$. The $\log_{10}$(MIPR) at various θ keeps zero in the region $r/t < 1$ and are finite numbers when $r/t > 1$, showing a phase transition at $r/t = 1$, namely, $\sqrt{V^2 + \lambda^2} = t$. Particularly, we note that the value of $\log_{10}$(MIPR) at $\theta = 0$ for $r/t > 1$ (corresponding to $V = 0$ and $\lambda > 1$) is significantly different from those for other θ's. The slightly smaller finite value of $\log_{10}$(MIPR) shows the critical characteristic of the system at these parameter points. The results are self-consistent with the fractional dimension discussed below. From the above analysis, the complete phase boundary is described by

$$\begin{aligned} V^2 + \lambda^2 &= t^2, \quad && V \neq 0, \\ \lambda &> t, && V = 0. \end{aligned} \tag{4}$$

However, in the axis of ordinates, for $\lambda = 0t$ and $V > t$, the system is in the localized phase. As a result, the phase boundary $V^2 + \lambda^2 = t^2$ in Fig. 1 by the red dashed line is due to the numerical simulations. The exact phase boundary in the present Hamiltonian system is still elusive, while it can be analytically determined in some systems of quasidisorder, for example, for the system of mobility edges by the self-duality condition [21] and for the system of the topological phase transitions by the open and close of the energy gap [12].

We then use the fractional dimension β to validate the arguments made previously regarding the various phases. For a system with $L = F_m$ (F_m is the mth Fibonacci number), the fractional dimension at lattice site n, i.e., β_n can be extracted from

$$p_n = F_m^{-\beta_n}, \tag{5}$$

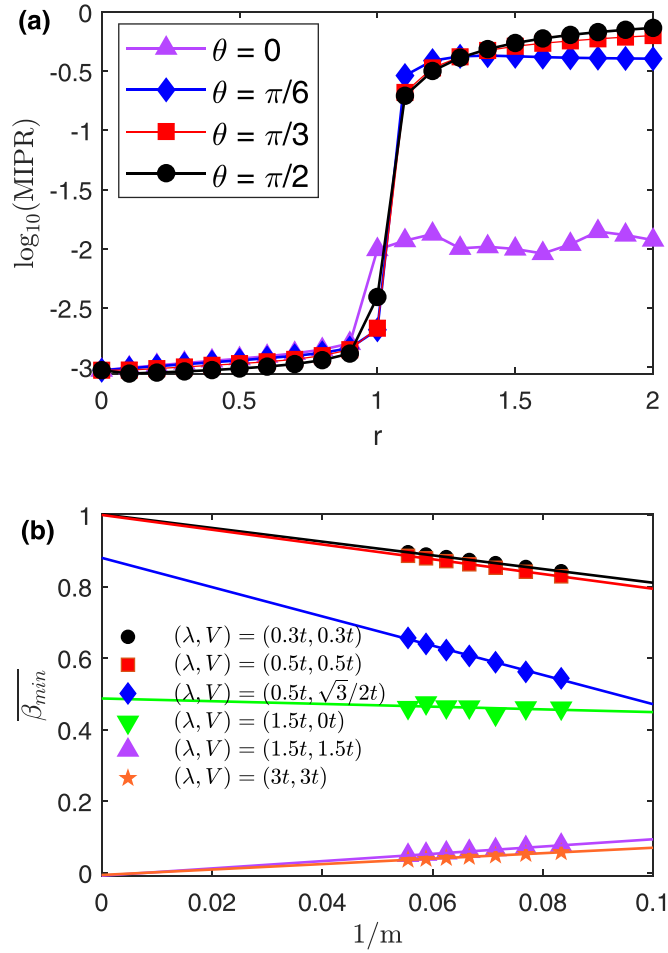

FIG. 3. (a) $\log_{10}$(MIPR) as a function of r with $\theta = 0, \pi/6, \pi/3, \pi/2$. (b) $\overline{\beta_{\min}}$ as a function of the inverse Fibonacci index $1/m$ at different (λ, V). Parameter points $(\lambda, V) = (0.3t, 0.3t)$ and $(0.5t, 0.5t)$ are chosen from the extended phase, $(\lambda, V) = (0.5t, \sqrt{3}/2t)$ and $(1.5t, 0t)$ are chosen from the critical phase, and $(\lambda, V) = (1.5t, 1.5t), (3t, 3t)$ are located in the localized phase.

where p_n is the probability density. From the above equation, we know that this quantity β_n plays the role of a scaling index. $\beta_n \sim 1$ for an extended state since $p_n \sim 1/F_m$. For a localized state, $\beta_n \sim 1$ on those localized sites and $\beta_n \to \infty$ on the other unoccupied sites. For a critical state, the index β_n is within a finite interval $[\beta^n_{\min}, \beta^n_{\max}]$. As a result, the minimal β_n, i.e., $\beta^n_{\min}$, is a direct feedback of the characteristic of a designated wave function [47]. Specifically, $\beta^n_{\min} \to 0$ signals a localized state, $0 < \beta^n_{\min} < 1$ a critical state, and $\beta^n_{\min} \to 1$ an extended state. Without loss of generality, we employ the average of $\beta^n_{\min}$ over all states, i.e., $\overline{\beta_{\min}} = \sum_i \beta^i_{\min}/L$ under the extrapolation limit $1/m \to 0$ to distinguish different phases. We choose some typical parameter points in various phases to calculate the $\overline{\beta_{min}}$. As shown in Fig. 3(b), we find that the corresponding $\overline{\beta_{\min}}$ tends to 1 at both $(\lambda, V) = (0.3t, 0.3t)$ and $(0.5t, 0.5t)$, verifying that the system is in the extended phase. As predicted, the corresponding $\overline{\beta_{\min}}$ approaches the value within (0,1) in the thermodynamic limit at both $(\lambda, V) = (0.5t, \sqrt{3}/2t)$ and $(1.5t, 0t)$, showing the distinctly critical characteristics. At $(\lambda, V) = (1.5t, 1.5t)$ and $(3t, 3t)$, the

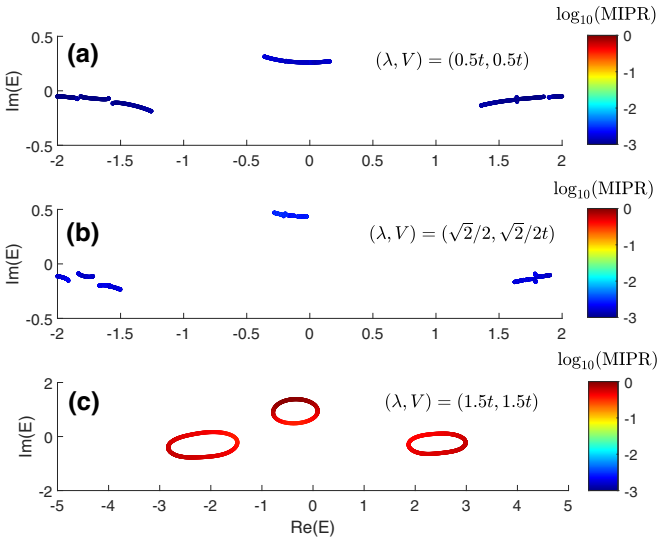

FIG. 4. Real energy spectrum of the incommensurate modulation case shown in the complex plane with (a) $(\lambda, V) = (0.5t, 0.5t)$; (b) $(\lambda, V) = (\sqrt{2}/2t, \sqrt{2}/2t)$; and (c) $(\lambda, V) = (1.5t, 1.5t)$. The color bar is for the value of $\log_{10}$(MIPR). The system size is $L = 1597$.

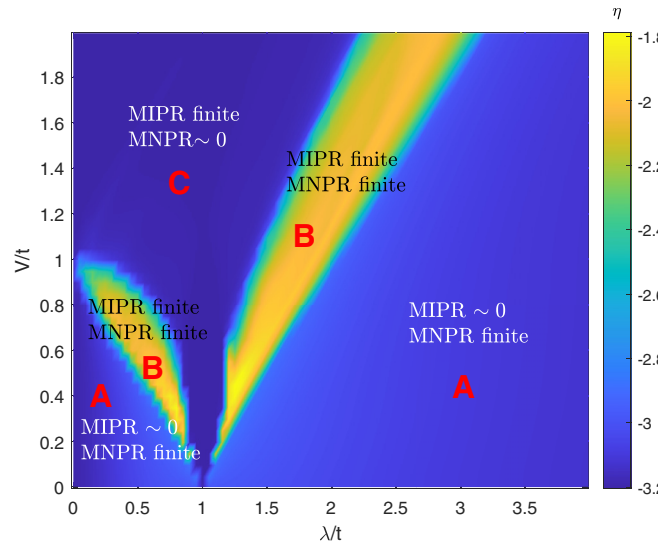

FIG. 5. Phase diagram of the commensurate modulation case presents η as a function of the parameters λ and V with the system size $L = 1597$. There are three different phases. Region B is the intermediate phase with $-2 \leqslant \eta \leqslant -1$, where both MIPR and MNPR are finite, and $\mathrm{Im}(E) \neq 0$. Region A is surrounded by region B and the X axis and indicates an extended phase and a pure real energy spectrum with $\eta < -3$, where MIPR is finite and MNPR ~ 0, and $\mathrm{Im}(E) \neq 0$. The rest of the phase diagram is reigion C, where the energy spectrum is complex and the wave function is localized with $\eta < -3$. MIPR ~ 0 and MNPR is finite, and $\mathrm{Im}(E) = 0$. The color bar is for the value of η.

corresponding $\overline{\beta_{\min}}$ extrapolates to 0, identifying that the system is in the localized phase.

In Ref. [29], there is a strict correspondence between the delocalization-localization transition and the real-complex transition, and the energy spectra in the complex plane is an ellipse symmetric about $\mathrm{Im}(E) = 0$, which means that the complex energies come in the form of conjugate pairs. The reason for this phenomenon is that the Hamiltonian is $\mathcal{PT}$ symmetric and as the strength of the non-Hermitian term changes, it undergoes a transition from a $\mathcal{PT}$-symmetric phase to a $\mathcal{PT}$-broken one. The off-diagonal incommensurate hopping modulation studied in this paper, breaks the $\mathcal{PT}$ symmetry. Hence, such a correspondence may not exist. Take parameter points $(\lambda, V) = (0.5t, 0.5t)$, $(\sqrt{2}/2t, \sqrt{2}/2t)$, and $(1.5t, 1.5t)$ corresponding to the extended phase, the critical phase at the boundary, and the localized phase. The corresponding energy spectra are plotted in Figs. 4(a), 4(b), and 4(c), respectively. Intuitively, all energy spectra are complex. Thus, there is no real-complex transition of the energy spectra accompanying the delocalization-localization phase transition. Moreover, the energy spectrum on the complex plane is not symmetric about $\mathrm{Im}(E) = 0$, due to the destruction of the $\mathcal{PT}$ symmetry. As a result, the strict correspondence between the delocalization-localization transition and the real-complex transition is not robust and broken by the off-diagonal incommensurate hopping modulation.

Besides the broken correspondence between the delocalization-localization transition and the real-complex transition, we notice that the energy spectra form open arms both in the extended and the critical phases, whereas in the localized phases, the energy spectra remain the closed loops. This situation is quite different from the present results in Refs. [29,30]. In these papers, there is a conventional correspondence among arc-loop shape, real-complex spectra, and delocalized-localized transitions. Although the real-complex transition is broken down, the correspondence between arc-loop shape and real-complex spectra is still preserved.

IV. COMMENSURATE MODULATION CASE

Now we focus on the commensurate modulation case. Without loss of generality, we choose $b_1 = 1/2$. The novel effective quantity η, suggested by Li and Das Sarma [48], is used in the numerical analyses and given by

$$\eta = \log_{10}[\mathrm{MIPR} \times \mathrm{MNPR}], \tag{6}$$

where MNPR is the abbreviation for the mean of the normalized participation ratio, which is the normalized participation ratio (NPR) averaged over all eigenstates $\mathrm{MNPR} = \sum_{j=1}^{L} \mathrm{NPR}^{(j)}/L$ with $\mathrm{NPR}^{(j)}$ defined as

$$\mathrm{NPR}^{j} = \left[L \frac{\sum_{n=1}^{L} |\psi^{(j)}(n)|^4}{\sum_{n=1}^{L} |\psi^{(j)}(n)|^2} \right]^{-1}, \tag{7}$$

used for separating the intermediate phase from the extended and localized ones. In the intermediate phase, both quantities of MIPR and MNPR are finite [$\sim \mathcal{O}(1)$], leading to $-2 \leqslant \eta \leqslant -1$. In the extended or localized phase, one of the two quantities scales as $\sim L^{-1}$, leading to $\eta < -\log_{10} L \sim -3$. By calculating η, the full phase diagram of the commensurate modulation case with $L = 1597$ ($\sim 10^3$) is depicted in Fig. 5. Intuitively, the phase diagram consists of two main regions. The region highlighted in blue, is marked by A or C, with η

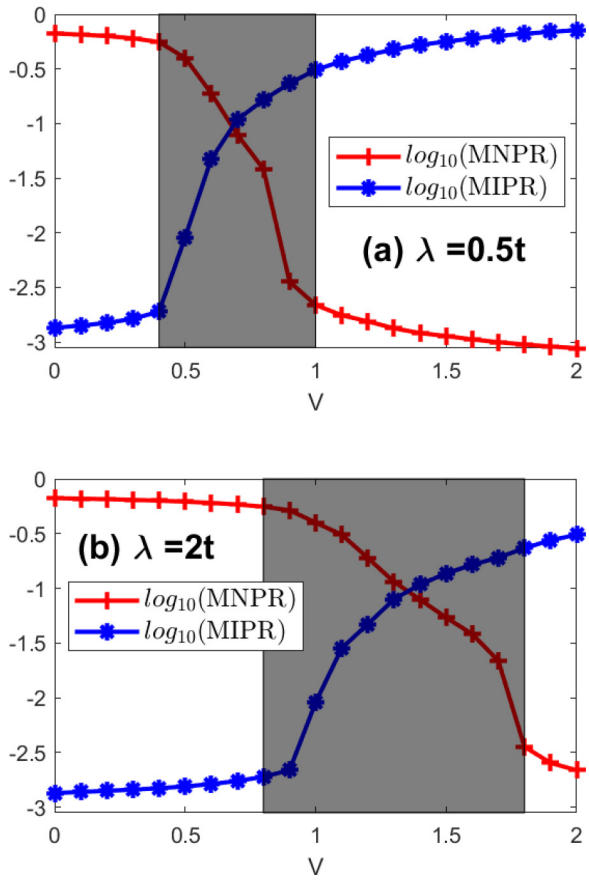

FIG. 6. $\log_{10}$(MNPR) and $\log_{10}$(MIPR) versus V/t in the case of the commensurate modulation $b_1 = 1/2$ for (a) $\lambda = 0.5t$ and (b) $2t$. The shaded area shows the intermediate phases. The system size is $L = 1597$.

less than -3, which is further distinguished by MNPR and MIPR. The other region has the value of η slightly larger: $-2 \leqslant \eta \leqslant -1$, marked by B, corresponding to the intermediate phase.

Now we further distinguish the regions A and C. Taking $\lambda = 0.5$ as an example, $\log_{10}$(MNPR) and $\log_{10}$(MNPR) as a function of the potential strength V are plotted in Fig. 6. Clearly, as V increases, the system undergoes the extended [MNPR $\sim \mathcal{O}(1)$ and NIPR $\sim L^{-1}$], intermediate [MNPR $\sim \mathcal{O}(1)$ and MIPR $\sim \mathcal{O}(1)$], and localized [MNPR $\sim L^{-1}$ and MIPR $\sim \mathcal{O}(1)$] phases. With this distinct definition, we make it clear that the blue region in Fig. 5 consists of the extended phase (marked by A) and the localized phase (marked by C).

In the case of the commensurate modulation, with the recovery of the $\mathcal{PT}$ symmetry, we find that the correspondence between the delocalization-localization phase transition and the real-complex transition in energy reappears. Taking the parameter point $(\lambda, V) = (0.5t, 0.1t)$ in the extended phase as an example, the energy spectrum is plotted in Fig. 7(a), from which we see that the energies are all real with $\log_{10}$(IPR) ~ -3. Figure 7(b) is the density distribution of the extended wave function $\psi^{(100)}$. On the contrary, at the parameter point $(\lambda, V) = (1t, 0.5t)$ taken from the localized phase, the corresponding energies are complex with $\log_{10}$(IPR) ~ 0, shown in Fig. 7(c). Figure 7(d) presents the localized density distribution of the wave function $\psi^{(100)}$.

Meanwhile, in the intermediate phase, the aforementioned correspondence still exists. Figure 8 presents the energy spectrum under $(\lambda, V) = (0.5t, 0.7t)$ (taken from the intermediate phase) with $L = 1597$. Intuitively, the energies of the extended states with $\log_{10}$(IPR) ~ -3 are all real and those of the localized states with $\log_{10}$(IPR) larger than -3 are fully complex. Thus, in this situation, we obtain the non-Hermitian mobility edges, characterized by the real and complex parts of the energy spectrum corresponding to the extended and localized states, respectively. And because of the $\mathcal{PT}$ symmetry (see the Appendix), complex energies always appear in the form of conjugate pairs [also as in Fig. 7(c)] and the appearance of the real energy is associated with the mobility edge.

To further explore the details of the mobility edge, we present the distributions of IPRs for the systems with $(\lambda, V) = (0.5t, 0.7t)$ and $(\lambda, V) = (2t, 1.5t)$ in Fig. 9. The states are arranged in ascending order of the real parts of the energies. In the mixed phase, the IPR varies from a finite value to $1/L$, and the sudden changes in the distributions of the IPRs indicate the presence of a mobility edge. In Fig. 10, we show the representative spatial density distributions for the systems with $(\lambda, V) = (0.5t, 0.7t)$ and $L = 1597$, and the corresponding energy spectra are plotted in Fig. 8. Figure 10(a) shows the localized states with complex energy and its real part $\mathrm{Re}(E) \sim 0.94t$ (taken from the bigger energy loop in Fig. 8) and 10(b) the localized states with $\mathrm{Re}(E) \sim 1.51t$ (the smaller energy loop in Fig. 8). Figure 10(c) shows one of the extended states with real energy $E \sim 1.62t$ (corresponding to the real energy spectra in Fig. 8).

V. SUMMARY

In this work, we have numerically studied a generalized Aubry-André-Harper model with off-diagonal incommensurate or commensurate hoppings and non-Hermitian exponential potential. The correspondence between the real-complex transition and the delocalization-localization transition is missing due to the incommensurate off-diagonal modulations, which breaks the $\mathcal{PT}$ symmetry. In addition, we find that for the incommensurate hopping, the phase diagram shows that the extended phase and the localized one are separated by the phase boundary $V^2 + \lambda^2 = t^2$. The extended phase forms a quarter-circle area in the positive-definite parameter region. The extended-localized transition is self-consistently analyzed by the MIPR and fractal dimension. For the commensurate hopping case, there appears an extra intermediate phase, which has the non-Hermitian mobility edge, which splits the real and complex parts of the energy spectrum and simultaneously the extended and localized states. Due to the recovery of the $\mathcal{PT}$ symmetry, separated by the mobility edge, we find that the correspondence between the real-complex transition in energy and the delocalization-localization phase transition reappears.

We notice that a generalized AAH model with both diagonal and off-diagonal quasiperiodic disorders is recently realized by the technique of momentum-lattice engineering in the ultracold atomic system [18,24], where the topological phase with the critical localization in a quasiperiodic

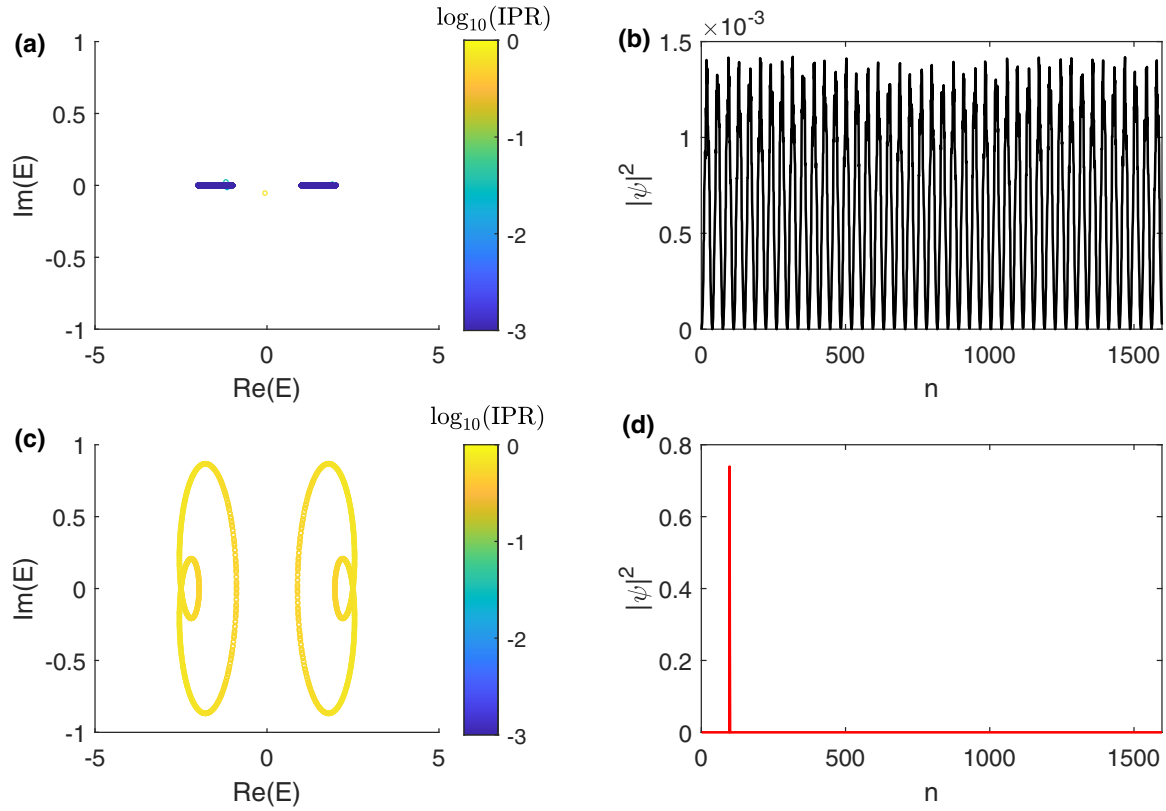

FIG. 7. (a) Real energy spectrum of the commensurate modulation case shown in the complex plane with $(\lambda, V) = (0.5t, 0.1t)$. The color bar is $\log_{10}$(IPR). (b) Spatial distribution of the wave function $\psi^{(100)}$ at $(\lambda, V) = (0.5t, 0.1t)$. (c) Complex energy spectrum shown in the complex plane at $(\lambda, V) = (0.5t, 1t)$. The color bar is $\log_{10}$(IPR). (d) Spatial distribution of the wave function $\psi^{(100)}$ at $(\lambda, V) = (0.5t, 1t)$. The color bar is for the value of $\log_{10}$(IPR). Another involved parameter is $L = 1597$.

lattice is observed. In the experimental implementation of Ref. [18], ^{87}Rb atoms are confined in a one-dimensional momentum lattice. Due to a series of frequency-modulated Bragg-laser pairs, the discrete momentum states of the atoms are coupled together. Once the Bragg-coupling parameters between nearest-neighbor sites are adjusted, both the diagonal and off-diagonal disorders are imposed. In addition, the complex quasiperiodic on-site potential can be realized by a

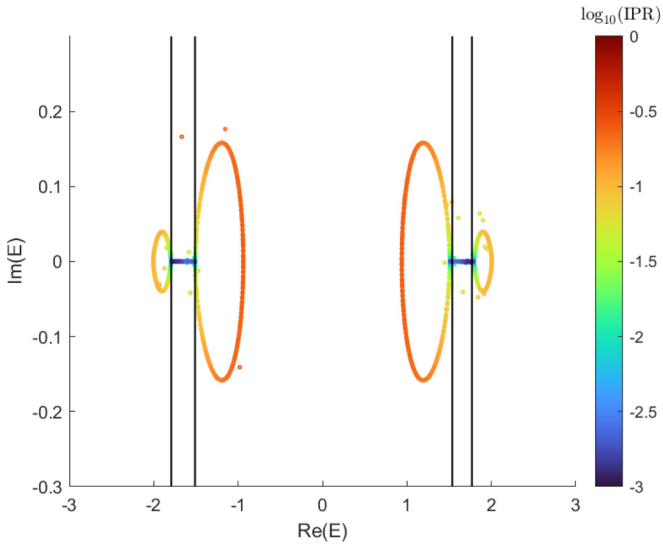

FIG. 8. Energy spectrum of the commensurate modulation case plotted in the complex plane with $(\lambda, V) = (0.5t, 0.7t)$ and $L = 1597$. The black dashed lines are mobility edges. The color bar shows the value of $\log_{10}$(IPR).

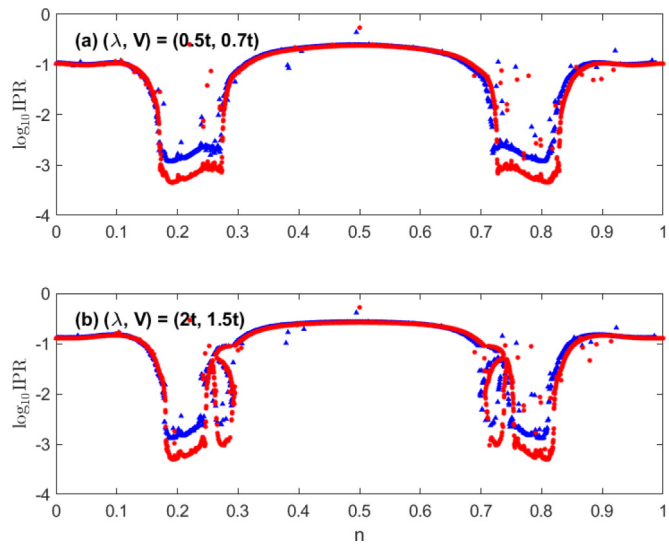

FIG. 9. Distributions of the IPRs for the systems with (a) $(\lambda, V) = (0.5t, 0.7t)$ and (b) $(\lambda, V) = (2t, 1.5t)$. Red points and blue triangles correspond to the results under different system size, $L = 1597$ and $L = 4181$.

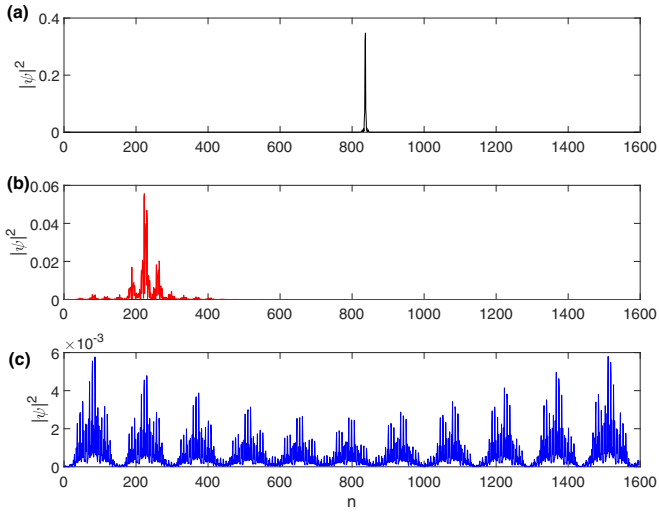

FIG. 10. The representative wave functions for the systems with $(\lambda, V) = (0.5t, 0.7t)$ and $L = 1597$. (a) $\mathrm{Re}(E) \approx 0.94$; (b) $\mathrm{Re}(E) \approx 1.51$; (c) $\mathrm{Re}(E) \approx 1.62$, corresponding to the eigenstates in the complex plane in Fig. 8.

low-finesse intracavity etalon, with free spectral range incommensurate with respect to the modulation frequency and much smaller than the gain bandwidth [30]. In addition, excellent experimental progress has been made in the observation of the topological triple phase transition in non-Hermitian Floquet quasicrystals via photonic quantum walks [49]. As a result, we believe that the breakdown of the correspondence between the real-complex and delocalization-localization transitions for the model we studied here has the potential to be realized in cold atomic experiments or in photonic quantum walks.

ACKNOWLEDGMENTS

The authors acknowledge support from NSFC under Grants No. 11835011 and No. 12174346. R.A. thanks R. R. Tabar for fruitful discussions.

APPENDIX: SYMMETRIES OF THE SYSTEM

The effects of parity operator $\hat{\mathcal{P}}$ and time-reversal operator $\hat{\mathcal{T}}$ on discrete systems are as follows:

$$\hat{\mathcal{P}}\hat{c}_n^\dagger\hat{\mathcal{P}} = \hat{c}_{L+1-n}^\dagger, \quad \hat{\mathcal{T}}i\hat{\mathcal{T}} = -i. \tag{A1}$$

And the Hamiltonian [see Eq. (4)] can be expressed as

$$\hat{H} = \hat{H}_{\text{hopping}} + \hat{H}_{\text{potential}}. \tag{A2}$$

First, we consider the non-Hermitian quasiperiodic potential,

$$\hat{H}_{\text{potential}} = \sum_n^L \exp\left[i(2\pi b_2 n + \phi_2)\right]\hat{c}_n^\dagger\hat{c}_n. \tag{A3}$$

Under the $\hat{\mathcal{P}}\hat{\mathcal{T}}$ operator,

$$\begin{aligned}
&\hat{\mathcal{P}}\hat{\mathcal{T}}\hat{H}_{\text{potential}}\hat{\mathcal{T}}\hat{\mathcal{P}} \\
&= \hat{\mathcal{P}}\hat{\mathcal{T}}\sum_n^L \exp\left[i(2\pi b_2 n + \phi_2)\right]\hat{c}_n^\dagger\hat{c}_n\hat{\mathcal{T}}\hat{\mathcal{P}} \\
&= \sum_n^L \{\cos\left[2\pi b_2(L-n+1) - 2\pi b_2(L+1) - \phi_2\right] \\
&\quad + i\sin\left[2\pi b_2(L-n+1) - 2\pi b_2(L+1) - \phi_2\right]\} \\
&\quad \times \hat{c}_{L-n+1}^\dagger\hat{c}_{L-n+1}.
\end{aligned} \tag{A4}$$

And then we deal with the hopping terms

$$\hat{H}_{\text{hopping}} = \sum_n^{L-1}[t + \lambda\cos(2\pi b_1 n + \phi_1)](\hat{c}_{n+1}^\dagger\hat{c}_n + \text{H.c.}). \tag{A5}$$

Applying the $\hat{\mathcal{P}}\hat{\mathcal{T}}$ operator on hopping terms,

$$\begin{aligned}
&\hat{\mathcal{P}}\hat{\mathcal{T}}\hat{H}_{\text{hopping}}\hat{\mathcal{T}}\hat{\mathcal{P}} \\
&= \hat{\mathcal{P}}\hat{\mathcal{T}}\sum_n^{L-1}[t + \lambda\cos(2\pi b_1 n + \phi_1)](\hat{c}_{n+1}^\dagger\hat{c}_n + \text{H.c.})\hat{\mathcal{T}}\hat{\mathcal{P}} \\
&= \sum_n^{L-1}[t + \lambda\cos(2\pi b_1 n + \phi_1)](\hat{c}_{L-n}^\dagger\hat{c}_{L-n+1} + \hat{c}_{L-n+1}^\dagger\hat{c}_{L-n}) \\
&= \sum_n^{L-1}\{t + \lambda\cos\left[2\pi b_1(L-n) - 2\pi b_1 L - \phi_1\right]\} \\
&\quad \times (\hat{c}_{L-n}^\dagger\hat{c}_{L-n+1} + \hat{c}_{L-n+1}^\dagger\hat{c}_{L-n}).
\end{aligned} \tag{A6}$$

The $\hat{\mathcal{P}}\hat{\mathcal{T}}$ symmetry is observed,

$$\hat{\mathcal{P}}\hat{\mathcal{T}}\hat{H}(\phi_1, \phi_2)\hat{\mathcal{T}}\hat{\mathcal{P}} = \hat{H}(\phi_1, \phi_2), \tag{A7}$$

when $\tilde{\phi}_1 \equiv -2\pi b_1 L - \phi_1$ and $\tilde{\phi}_2 \equiv -2\pi b_2(L+1) - \phi_2$ satisfy

$$\tilde{\phi}_1 = -2\pi b_1 L - \phi_1 = \phi_1 + 2k_1\pi, \tag{A8}$$

$$\tilde{\phi}_2 = -2\pi b_2(L+1) - \phi_2 = \phi_2 + 2k_2\pi, \tag{A9}$$

namely,

$$\phi_1 = -\pi b_1 L - k_1\pi, \quad k_1 \in Z, \tag{A10}$$

$$\phi_2 = -\pi b_2(L+1) - k_2\pi, \quad k_2 \in Z. \tag{A11}$$

In this case, the system is invariant under the $\hat{\mathcal{P}}\hat{\mathcal{T}}$ operator.

In order to ensure that the systems satisfy $\mathcal{PT}$ symmetry at any phase factor, we need to construct a new antiunitary operator $\hat{\mathcal{R}}\hat{\mathcal{P}}\hat{\mathcal{T}}$, and the eigenenergy spectrum of the system is invariant under the $\hat{\mathcal{R}}$ transformations [50,51]. If b_1 is rational, and the strength of the hopping terms between sites are periodic, we can construct a unitary operator rotating the system by Mk' sites in the counterclockwise direction,

$$\hat{\mathcal{R}}_{k'}^\dagger\hat{c}_n^\dagger\hat{\mathcal{R}}_{k'} = \hat{c}_{n+Mk'}^\dagger, \tag{A12}$$

where M is the periodic of the hopping term. It gives

$$\tilde{\phi}_1' = \tilde{\phi}_1 - \frac{2\pi Mk'}{L}, \tag{A13}$$

$$\tilde{\phi}_2' = \tilde{\phi}_2 - \frac{2\pi Mk'}{L}, \tag{A14}$$

and Hamiltonian under the rotation operators R_k,

$$\hat{\mathcal{R}}_{k'}^{\dagger}\hat{H}(\tilde{\phi}_1,\tilde{\phi}_2)\hat{\mathcal{R}}_{k'}=\hat{H}(\tilde{\phi}_1',\tilde{\phi}_2'), \tag{A15}$$

have the same eigenenergy spectra because $\hat{\mathcal{R}}_k$ is unitary. So if systems have $\hat{\mathcal{P}}\hat{\mathcal{T}}$ symmetry, phase factors ϕ_1 and ϕ_2 satisfy

$$\tilde{\phi}_1'=\tilde{\phi}_1-\frac{2\pi Mk'}{L}=\phi_1+2k_1\pi, \tag{A16}$$

$$\tilde{\phi}_2'=\tilde{\phi}_2-\frac{2\pi Mk'}{L}=\phi_2+2k_2\pi, \tag{A17}$$

namely,

$$\phi_1=-\pi b_1L-k_1\pi+\frac{k'\pi M}{L},\quad k_1,k'\in Z, \tag{A18}$$

$$\phi_2=-\pi b_2(L+1)-k_2\pi+\frac{k'\pi M}{L},\quad k_2,k'\in Z, \tag{A19}$$

and the number of points satisfying the condition above becomes infinite for $L\to\infty$. So in the thermodynamic limit, if b_1 is rational, systems have $\hat{\mathcal{P}}\hat{\mathcal{T}}$ symmetry. On the other hand, if b_1 is irrational, the systems do not have rotation symmetry so the $\hat{\mathcal{P}}\hat{\mathcal{T}}$ symmetry is broken.

[1] P. W. Anderson, Absence of diffusion in certain random lattices, Phys. Rev. **109**, 1492 (1958).

[2] E. Abrahams, P. W. Anderson, D. C. Licciardello, and T. V. Ramakrishnan, Scaling Theory of Localization: Absence of Quantum Diffusion in Two Dimensions, Phys. Rev. Lett. **42**, 673 (1979).

[3] T. Guhr, A. Müller-Groeling, and H. A. Weidenmüller, Random-matrix theories in quantum physics: common concepts, Phys. Rep. **299**, 189 (1998).

[4] B. Kramer and A. MacKinnon, Localization: Theory and experiment, Rep. Prog. Phys. **56**, 1469 (1993).

[5] S. Aubry and G. André, Analyticity breaking and Anderson localization in incommensurate lattices, Ann. Israel Phys. Soc **3**, 18 (1980).

[6] P. G. Harper, Single band motion of conduction electrons in a uniform magnetic field, Proc. Phys. Soc., London, Sect. A **68**, 874 (1955).

[7] K. A. Madsen, E. J. Bergholtz, and P. W. Brouwer, Topological equivalence of crystal and quasicrystal band structures, Phys. Rev. B **88**, 125118 (2013).

[8] L.-J. Lang, X. Cai, and S. Chen, Edge States and Topological Phases in One-Dimensional Optical Superlattices, Phys. Rev. Lett. **108**, 220401 (2012).

[9] J. Vidal, D. Mouhanna, and T. Giamarchi, Correlated Fermions in a One-Dimensional Quasiperiodic Potential, Phys. Rev. Lett. **83**, 3908 (1999).

[10] Y. E. Kraus and O. Zilberberg, Topological Equivalence between the Fibonacci Quasicrystal and the Harper Model, Phys. Rev. Lett. **109**, 116404 (2012).

[11] S. Ganeshan, K. Sun, and S. Das Sarma, Topological Zero-Energy Modes in Gapless Commensurate Aubry-André-Harper Models, Phys. Rev. Lett. **110**, 180403 (2013).

[12] F. Liu, S. Ghosh, and Y. D. Chong, Localization and adiabatic pumping in a generalized Aubry-André-Harper model, Phys. Rev. B **91**, 014108 (2015).

[13] Q.-B. Zeng, Y.-B. Yang, and R. Lü, Topological phases in one-dimensional nonreciprocal superlattices, Phys. Rev. B **101**, 125418 (2020).

[14] Y. Lahini, R. Pugatch, F. Pozzi, M. Sorel, R. Morandotti, N. Davidson, and Y. Silberberg, Observation of a Localization Transition in Quasiperiodic Photonic Lattices, Phys. Rev. Lett. **103**, 013901 (2009).

[15] M. Verbin, O. Zilberberg, Y. E. Kraus, Y. Lahini, and Y. Silberberg, Observation of Topological Phase Transitions in Photonic Quasicrystals, Phys. Rev. Lett. **110**, 076403 (2013).

[16] Y. E. Kraus, Y. Lahini, Z. Ringel, M. Verbin, and O. Zilberberg, Topological States and Adiabatic Pumping in Quasicrystals, Phys. Rev. Lett. **109**, 106402 (2012).

[17] L. Dal Negro, C. J. Oton, Z. Gaburro, L. Pavesi, P. Johnson, A. Lagendijk, R. Righini, M. Colocci, and D. S. Wiersma, Light Transport through the Band-Edge States of Fibonacci Quasicrystals, Phys. Rev. Lett. **90**, 055501 (2003).

[18] T. Xiao, D. Xie, Z. Dong, T. Chen, W. Yi, and B. Yan, Observation of topological phase with critical localization in a quasi-periodic lattice, Sci. Bull. **66**, 2175 (2021).

[19] G. Roati, C. D'Errico, L. Fallani, M. Fattori, C. Fort, M. Zaccanti, G. Modugno, M. Modugno, and M. Inguscio, Anderson localization of a non-interacting Bose-Einstein condensate, Nature (London) **453**, 895 (2008).

[20] G. Modugno, Anderson localization in Bose–Einstein condensates, Rep. Prog. Phys. **73**, 102401 (2010).

[21] J. Biddle and S. Das Sarma, Predicted Mobility Edges in One-Dimensional Incommensurate Optical Lattices: An Exactly Solvable Model of Anderson Localization, Phys. Rev. Lett. **104**, 070601 (2010).

[22] T. Liu, H. Guo, Y. Pu, and S. Longhi, Generalized Aubry-André self-duality and mobility edges in non-Hermitian quasiperiodic lattices, Phys. Rev. B **102**, 024205 (2020).

[23] J. C. C. Cestari, A. Foerster, and M. A. Gusmão, Fate of topological states in incommensurate generalized Aubry-André models, Phys. Rev. B **93**, 205441 (2016).

[24] T. Liu, P. Wang, and G. Xianlong, Phase diagram of the off-diagonal Aubry-André model, arXiv:1609.06939.

[25] N. Hatano and D. R. Nelson, Localization Transitions in Non-Hermitian Quantum Mechanics, Phys. Rev. Lett. **77**, 570 (1996).

[26] S. Longhi, Non-Hermitian skin effect beyond the tight-binding models, Phys. Rev. B **104**, 125109 (2021).

[27] S. Longhi, Spectral deformations in non-Hermitian lattices with disorder and skin effect: A solvable model, Phys. Rev. B **103**, 144202 (2021).

[28] S. Longhi, Phase transitions in a non-Hermitian Aubry-André-Harper model, Phys. Rev. B **103**, 054203 (2021).

[29] S. Longhi, Metal-insulator phase transition in a non-Hermitian Aubry-André-Harper model, Phys. Rev. B **100**, 125157 (2019).

[30] S. Longhi, Topological Phase Transition in Non-Hermitian Quasicrystals, Phys. Rev. Lett. **122**, 237601 (2019).

[31] C. M. Bender and S. Boettcher, Real Spectra in Non-Hermitian Hamiltonians Having $\mathcal{PT}$ Symmetry, Phys. Rev. Lett. **80**, 5243 (1998).

[32] Q.-B. Zeng, S. Chen, and R. Lü, Anderson localization in the non-Hermitian Aubry-André-Harper model with physical gain and loss, Phys. Rev. A **95**, 062118 (2017).

[33] Z. Xu, Y. Zhang, and S. Chen, Topological phase transition and charge pumping in a one-dimensional periodically driven optical lattice, Phys. Rev. A **96**, 013606 (2017).

[34] Y. Liu, X.-P. Jiang, J. Cao, and S. Chen, Non-Hermitian mobility edges in one-dimensional quasicrystals with parity-time symmetry, Phys. Rev. B **101**, 174205 (2020).

[35] C.-X. Guo, C.-H. Liu, X.-M. Zhao, Y. Liu, and S. Chen, Exact Solution of Non-Hermitian Systems with Generalized Boundary Conditions: Size-Dependent Boundary Effect and Fragility of the Skin Effect, Phys. Rev. Lett. **127**, 116801 (2021).

[36] Y. Liu, Y. Zeng, L. Li, and S. Chen, Exact solution of the single impurity problem in nonreciprocal lattices: Impurity-induced size-dependent non-Hermitian skin effect, Phys. Rev. B **104**, 085401 (2021).

[37] Y. Liu, Y. Wang, Z. Zheng, and S. Chen, Exact non-Hermitian mobility edges in one-dimensional quasicrystal lattice with exponentially decaying hopping and its dual lattice, Phys. Rev. B **103**, 134208 (2021).

[38] Y. Liu, Y. Wang, X.-J. Liu, Q. Zhou, and S. Chen, Exact mobility edges, $\mathcal{PT}$-symmetry breaking, and skin effect in one-dimensional non-Hermitian quasicrystals, Phys. Rev. B **103**, 014203 (2021).

[39] Q.-B. Zeng, Y.-B. Yang, and Y. Xu, Topological phases in non-Hermitian Aubry-André-Harper models, Phys. Rev. B **101**, 020201(R) (2020).

[40] A. E. Bernardini and O. Bertolami, Generalized phase-space description of nonlinear Hamiltonian systems and Harper-like dynamics, Phys. Rev. A **105**, 032207 (2022).

[41] R. Hamazaki, K. Kawabata, and M. Ueda, Non-Hermitian Many-Body Localization, Phys. Rev. Lett. **123**, 090603 (2019).

[42] L.-Z. Tang, G.-Q. Zhang, L.-F. Zhang, and D.-W. Zhang, Localization and topological transitions in non-Hermitian quasiperiodic lattices, Phys. Rev. A **103**, 033325 (2021).

[43] J. Biddle, D. J. Priour, B. Wang, and S. Das Sarma, Localization in one-dimensional lattices with non-nearest-neighbor hopping: Generalized Anderson and Aubry-André models, Phys. Rev. B **83**, 075105 (2011).

[44] T. Liu, S. Cheng, H. Guo, and G. Xianlong, Fate of Majorana zero modes, exact location of critical states, and unconventional real-complex transition in non-Hermitian quasiperiodic lattices, Phys. Rev. B **103**, 104203 (2021).

[45] Y. V. Fyodorov and A. D. Mirlin, Level-to-Level Fluctuations of the Inverse Participation Ratio in Finite Quasi 1D Disordered Systems, Phys. Rev. Lett. **71**, 412 (1993).

[46] F. Evers and A. D. Mirlin, Fluctuations of the Inverse Participation Ratio at the Anderson Transition, Phys. Rev. Lett. **84**, 3690 (2000).

[47] J. Wang, X.-J. Liu, G. Xianlong, and H. Hu, Phase diagram of a non-Abelian Aubry-André-Harper model with p-wave superfluidity, Phys. Rev. B **93**, 104504 (2016).

[48] X. Li and S. Das Sarma, Mobility edge and intermediate phase in one-dimensional incommensurate lattice potentials, Phys. Rev. B **101**, 064203 (2020).

[49] S. Weidemann, M. Kremer, S. Longhi, and A. Szameit, Topological triple phase transition in non-Hermitian Floquet quasicrystals, Nature (London) **601**, 354 (2022).

[50] A. K. Harter, T. E. Lee, and Y. N. Joglekar, $\mathcal{PT}$-breaking threshold in spatially asymmetric Aubry-André and Harper models: Hidden symmetry and topological states, Phys. Rev. A **93**, 062101 (2016).

[51] S. Schiffer, X.-J. Liu, H. Hu, and J. Wang, Anderson localization transition in a robust $\mathcal{PT}$-symmetric phase of a generalized Aubry-André model, Phys. Rev. A **103**, L011302 (2021).